

Optimal probes for global quantum thermometry

Wai-Keong Mok¹, Kishor Bharti¹, Leong-Chuan Kwek ^{1,2,3,4} & Abolfazl Bayat⁵✉

Quantum thermodynamics has emerged as a separate sub-discipline, revising the concepts and laws of thermodynamics, at the quantum scale. In particular, there has been a disruptive shift in the way thermometry, and thermometers are perceived and designed. Currently, we face two major challenges in quantum thermometry. First, all of the existing optimally precise temperature probes are local, meaning their operation is optimal only for a narrow range of temperatures. Second, aforesaid optimal local probes mandate complex energy spectrum with immense degeneracy, rendering them impractical. Here, we address these challenges by formalizing the notion of global thermometry leading to the development of optimal temperature sensors over a wide range of temperatures. We observe the emergence of different phases for such optimal probes as the temperature interval is increased. In addition, we show how the best approximation of optimal global probes can be realized in spin chains, implementable in ion traps and quantum dots.

¹Centre for Quantum Technologies, National University of Singapore, Singapore, Singapore. ²MajuLab, CNRS-UNS-NUS-NTU International Joint Research Unit, Singapore, Singapore. ³National Institute of Education and Institute of Advanced Studies, Nanyang Technological University, Singapore, Singapore. ⁴School of Electrical and Electronic Engineering, Singapore, Singapore. ⁵Institute of Fundamental and Frontier Sciences, University of Electronic Science and Technology of China, Chengdu, China. ✉email: abolfazl.bayat@uestc.edu.cn

Recent advancements in quantum metrology^{1–3} have pushed the boundaries of thermodynamics into new territories, where small objects are cooled to ultra-low temperatures^{4,5}. This has led to the development of a fast-growing field of quantum thermodynamics^{6–9}. From a fundamental perspective, this provides revised definitions for some of the well-known concepts, such as work^{10,11} and heat¹², and extending the formulation for the laws of thermodynamics^{13–16} and scaling relations¹⁷ into the quantum regime. From a practical viewpoint, however, measuring the thermodynamic quantities at the quantum level mandates unprecedented precision¹⁸ and advanced refrigeration^{19–21}. Temperature, defined through the zeroth law of thermodynamics, is one of the key thermodynamical parameters, with its precise measurement having numerous applications from our daily life to almost any quantum experiment. Thermometry has been explored for near-term quantum simulators^{22,23} and various experimental platforms⁷, including nitrogen-vacancy (NV) centres in diamonds^{24,25}, optical nanofibres²⁶ and nano-photonic cavities coupled to nano-optomechanical resonators²⁷.

At low temperatures, precise temperature measurement is extremely challenging^{28–40}. To measure the temperature of a quantum system, one brings in a probe, i.e. thermometer, and interact it with the system. Then, the procedure of thermometry can be pursued in two ways: (i) non-equilibrium dynamics in which the temperature is extracted as a parameter from the state of the probe before its thermalization^{30,31,36,41–49}; and (ii) equilibrium approach in which the probe is measured after reaching an equilibrium with the system and, thus, is described by a thermal state with the same temperature as the system^{28,38,50–54}. In the first approach, the optimal measurement, which minimizes the uncertainty of the estimation through saturating the Cramér-Rao inequality⁵⁵, generally depends on the unknown temperature of the system which makes its achievement challenging in practice. In the second approach, which is the focus of this paper, the energy measurement is known to be the optimal choice which saturates the quantum Cramér-Rao bound²⁸ independent of temperature. Nonetheless, not all probes provide the same precision in equilibrium thermometry. Therefore, one may wonder what an optimal probe for equilibrium quantum thermometry is.

In a previous work⁵⁰, the above question has been answered analytically for a general N -level quantum probe. The result shows that the probe has to be an effective two-level system with a unique ground state and $N - 1$ degenerate excited states. Unlike the optimal measurement basis, the energy gap of the optimal probe is temperature-dependent. This means that the design of an optimal probe needs prior information about the temperature of the system. In other words, the probe can only be used for local thermometry in which the temperature is roughly known, and the objective of thermometry is just to measure it more precisely. Moreover, this optimal probe, with enormous degeneracy in its excited state, is very difficult to be realized in practice. Based on these, there are several natural questions that one can ask: (i) How can we design a probe which operates optimally over a wide range of temperatures? (ii) What does the optimal probe look like if one takes the practical constraints into account?

In this paper, we address all of the aforementioned questions. We first quantitatively develop the concept of global thermometry over an arbitrary temperature interval and introduce the average variance as the quantity which has to be minimized to get the optimal probe. Our notion of global thermometry is distinct from existing works in literature, where the word “global” refers to system size³⁷ and not temperature range. Using our approach, we can determine the optimal probe over a wide range of temperature intervals. We find that the structure of the optimal probe

goes through different phases, each with its own energy structure, as the temperature interval increases. We then focus on spin chain probes with various constraints to get the structure of the optimal probes considering practical limitations which one may face in realistic scenarios. Our results show that for the non-uniform XYZ Hamiltonians, the Ising spin chain provides the optimal probe. By considering the non-uniform Heisenberg Hamiltonians, the dimer spin chains become optimal. Our results pave the way for global thermometry in various physical systems, including ion traps and quantum dot arrays.

Results and discussion

Local quantum thermometry. In this section, we review the concept of local quantum thermometry at equilibrium and its optimal probes. Let us consider a thermometer that weakly interacts with a system at some temperature T (see scheme in Fig. 1a). At thermal equilibrium, we can assume that the probe thermalizes at the system temperature T , and is thus described by the Gibbs state $\rho_{\text{th}} = \exp(-\beta H_p)/\mathcal{Z}$, where $\beta \equiv 1/k_B T$ is the inverse temperature (we set $k_B = 1$ henceforth), H_p is the probe Hamiltonian with N eigenvalues and \mathcal{Z} is the partition function. For \mathcal{M} measurement samples, the variance in the estimation of temperature (see Fig. 1a) satisfies the Cramér-Rao inequality:

$$(\Delta T)^2 \geq \frac{1}{\mathcal{M} \mathcal{F}_{\text{th}}} \quad (1)$$

where \mathcal{F}_{th} is the thermal quantum Fisher information (QFI) at equilibrium, which can be related to the heat capacity and hence the energy variance of the probe⁷:

$$\mathcal{F}_{\text{th}} = \frac{(\Delta H_p)^2}{T^4} = \frac{\langle H_p^2 \rangle - \langle H_p \rangle^2}{T^4} \quad (2)$$

It is worth emphasizing that the Cramér-Rao bound is saturated for all temperatures if one measures the probe in the energy basis²⁸, for which ρ_{th} is diagonal. Thus, in equilibrium thermometry, the only way to increase precision is by increasing the thermal QFI through proper engineering of the probe. However, \mathcal{F}_{th} depends on the actual energy spectrum of the probe. An interesting question then arises: what is the optimal Hamiltonian spectrum for a N -level system that maximizes the thermal QFI? This question was answered in a previous work by Correa et al.⁵⁰, where they proved that the optimal energy spectrum is an effective two-level system with a single ground state and a $(N - 1)$ -fold degenerate excited state. They also showed that the energy gap ϵ between the excited state and ground state is the solution of a transcendental equation⁵⁰:

$$e^x = (N - 1) \frac{x + 2}{x - 2} \quad (3)$$

where $x \equiv \epsilon/T$ is the dimensionless energy gap.

Nonetheless, this optimal thermometry has a serious limitation as from Eq. (3), one can only obtain the ratio ϵ/T . Hence, for a fixed number of energy levels N , the optimal energy gap ϵ scales linearly with the temperature T . However, T is generally unknown to us. Thus, the probe cannot be optimized unless the temperature is already known within a narrow range, which limits the usefulness of the probe. Due to this limitation, this scheme is known as local thermometry.

Global quantum thermometry. In order to go beyond the limitations of local thermometry, one has to first define the paradigm of global thermometry in which the probe can operate optimally over a wide range of temperatures. We define the average

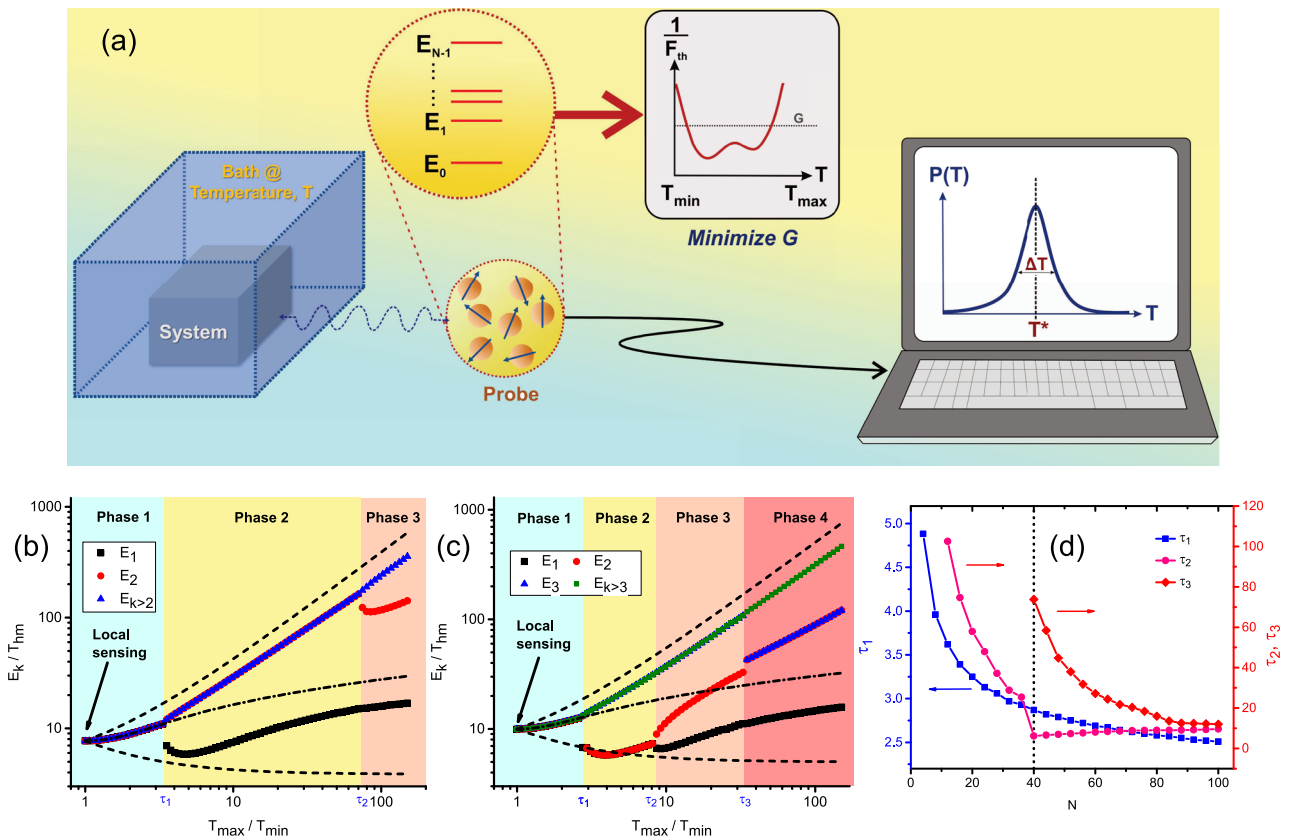


Fig. 1 Global quantum thermometry. **a** Schematic of our proposal. A probe weakly interacts with the system and thus reaches an equilibrium at the system temperature $T \in [T_{\min}, T_{\max}]$. The probe equilibrium state is characterized by a certain energy spectrum with levels E_0, \dots, E_{N-1} with N being the number of energy levels. The energy spectrum also determines the thermal quantum Fisher information \mathcal{F}_{th} as a function of T . The global thermometry measure G , defined in Eq. (4) as the average uncertainty of the probe, is a property of the probe energy spectrum, and is minimized to achieve the optimal probe. Energy measurements on the probe yield a probability distribution of temperatures with an estimated temperature T^* and variance $(\Delta T)^2$. The optimal energies against temperature ratio T_{\max}/T_{\min} for a general N -level system are obtained for: **b** $N = 16$, with $E_{k>2}$ denoting the degenerate energy levels $E_3 = \dots = E_{N-1}$. **c** $N = 64$, with $E_{k>3}$ denoting the degenerate energy levels $E_4 = \dots = E_{N-1}$. In **(b)** and **(c)**, the energies are scaled with the characteristic temperature T_{hm} , where T_{hm} is the harmonic mean of T_{\min} and T_{\max} . The leftmost data point corresponds to the case of the locally optimal thermometer. The dashed lines indicate the approximate bounds for the energies (explained in main text), while the dash-dotted line shows the optimal energy gap for an effective two-level system. **d** Critical ratios τ_k against N . The critical ratios correspond to the temperature ratios T_{\max}/T_{\min} at the boundaries of two phases, as labelled in **(b)** and **(c)**.

variance $G(T_{\max}, T_{\min})$ over some given temperature range $[T_{\min}, T_{\max}]$ as

$$G(T_{\max}, T_{\min}) \equiv \frac{1}{T_{\max} - T_{\min}} \int_{T_{\min}}^{T_{\max}} \frac{dT}{\mathcal{F}_{\text{th}}(T)} \quad (4)$$

where the right-hand side is proportional to the average of Cramér-Rao bound in Eq. (1). Unlike the local thermometry scheme, in which the QFI is maximized, in the global thermometry one has to minimize the average variance $G(T_{\max}, T_{\min})$. In the limit of $T_{\max}/T_{\min} \rightarrow 1$, $G \rightarrow 1/\mathcal{F}_{\text{th}}$, and the minimization of G becomes equivalent to maximizing \mathcal{F}_{th} . This recovers the special case of local thermometry. The temperature estimation can also be done adaptively in the sense that once the temperature is estimated for a given range then one can then use a secondary probe optimized for a tighter range to get a better estimate. This procedure can be repeated until the desired precision is achieved.

For a given probe of size N , one has to optimize the $N - 1$ energy levels to minimize $G(T_{\max}, T_{\min})$, setting the ground state energy $E_0 = 0$ as a reference point. The aforementioned integral in Eq. (4) is very difficult to compute analytically (see Supplementary Note 1 for some analytical approximations), so

we use numerical optimization to minimize G over all the $N - 1$ independent energy levels. We note that for large system sizes, especially for the spin chains, the optimization routine becomes infeasible due to the computational costs from diagonalizing the Hamiltonian and the large number of iterations required to ensure a global optimum. In such cases, we combine local optimization with transfer learning to speed up the convergence to optimality (see “Methods” for more details).

Figure 1b, c shows the optimized energy spectrum for $N = 16$ and $N = 64$ energy levels, for a temperature range of up to $T_{\max}/T_{\min} = 150$. We use the harmonic mean temperature $T_{\text{hm}} \equiv (1/T_{\max} + 1/T_{\min})^{-1}$ as the characteristic temperature, and plot the energy levels normalized by T_{hm} against the temperature ratio T_{\max}/T_{\min} . Since the ground state is fixed to be $E_0 = 0$, we only plot the energy levels of the excited states, where E_k is the energy of the k th excited state. In the limiting case where $T_{\max}/T_{\min} = 1$, the situation reduces to the local thermometry case⁵⁰. Unsurprisingly, numerical optimization gives the energy gap $E_1 = E_2 = \dots = E_{N-1} \approx 7.708 T_{\text{hm}}$, which is consistent with Eq. (3). This exactly describes the effective two-level solution obtained for local thermometry⁵⁰. As the ratio T_{\max}/T_{\min} is increased further, the optimal solution is again an

effective two-level system with a $(N - 1)$ -fold degenerate excited state. We call this regime of the optimal energy spectrum, namely an effective two-level system, Phase 1. We use the term "phase" throughout the paper to refer to a range of temperature ratio T_{\max}/T_{\min} where the energy structure of the optimal probe is the same (e.g. effective two-level system). The energy gap here, of course, cannot be described by Eq. (3), as both T_{\min} and T_{\max} have to be taken into account. The corrections to Eq. (3) for the regime T_{\max}/T_{\min} near unity can be found in Supplementary Note 1.

The upper and lower dashed lines in Fig. 1b, c denotes the optimal energy gap when the probe is optimized for only T_{\max} or T_{\min} , respectively. This gives a nice physical intuition for the optimal energy gap, as a compromise between the locally optimal probes at T_{\max} and T_{\min} . A simple estimate of the energy gap is the average energy between the upper and lower bounds, which is equivalent to optimizing the probe at the average temperature $(T_{\max} + T_{\min})/2$. This is fairly accurate, within 3% of the actual energy gap in Phase 1 for $N = 16$.

As the temperature ratio T_{\max}/T_{\min} is increased beyond some critical ratio τ_1 , the optimal energy spectrum is no longer an effective two-level system. Instead, the energy levels remarkably bifurcate into two branches creating a new regime of energy spectrum, namely Phase 2. The optimal probe in Phase 2 is an effective three-level system. The dashed-dotted lines in Fig. 1b, c show the optimization results when the probe is constrained to an effective two-level system, and, can be thought of as an extrapolation of the Phase 1 solutions.

The bifurcation of energy levels can be physically interpreted as the case where the optimal probe has to be sensitive to both ends of the temperature range. When the range is small (i.e. T_{\max}/T_{\min} below the critical ratio), optimizing the probe at a temperature near the mean gives a sufficiently high \mathcal{F}_{th} at both ends of the range. The optimal solution is the highly-degenerate two-level system which has been previously found to be the most sensitive probe for local thermometry⁵⁰. This argument is obviously not true in the limit where the temperature range is large (i.e. T_{\max}/T_{\min} above the critical ratio), and the energy gaps have to be split up to produce an effective probe over the entire temperature range. The above intuition is supported by the dashed lines, corresponding to the optimized local probes at T_{\min} and T_{\max} , respectively, which provide approximate bounds for the actual energy levels.

The huge discrepancy between the degeneracies of E_1 and E_2 (1 vs $N - 2$) is consistent with previous findings³⁸. This is because the population of the higher excited states are exponentially suppressed, which in turn demands a significantly higher degeneracy in order to achieve a reasonable sensitivity at higher temperatures. As the temperature ratio is increased further, we get further bifurcations of the energy levels in Phases 3 and 4 at the critical ratios τ_2 and τ_3 respectively in Fig. 1c, leading to an effective four-level system. The difference in the bifurcation diagram can be intuitively understood: for a larger N , more energy levels can be split up from the upper branch to 'support' the lower temperatures without sacrificing too much sensitivity at higher temperatures. The critical ratios are plotted against N in Fig. 1d. An interesting observation is that the critical ratio τ_2 decreases sharply at $N = 40$, with the emergence of Phase 4 as indicated by the presence of τ_3 .

In short, we have discovered new phases of optimal solutions for global quantum thermometry, when the previously found effective two-level system is no longer ideal. This allows us to delineate global thermometry into various regimes. We also emphasize that our observations for the emergence of various phases for the optimal global probe are universal. In other words, it does not depend on the specific T_{\min} and T_{\max} , and only depends on the ratio T_{\max}/T_{\min} and the harmonic mean T_{hm} .

Realization of optimal probes. Before we study the optimization of various practical spin chain models, we first demonstrate that the optimal energy spectrum for Phase 1 thermometry, the effective two-level system, can be obtained from a generalized version of the classical (or longitudinal-field) Ising model. Consider the Hamiltonian for n spin-1/2 particles (i.e. $N = 2^n$):

$$H = \sum_{k=1}^n H_k \quad (5)$$

where

$$H_k = \sum_{\langle i_1, i_2, \dots, i_k \rangle} J_k^{i_1, i_2, \dots, i_k} \sigma_z^{i_1} \sigma_z^{i_2} \dots \sigma_z^{i_k} \quad (6)$$

is the k -local Hamiltonian with coupling parameters J_k (omitting the spin indices), and σ_z^i is the Pauli Z operator for the i th spin. For example, H_1 can be interpreted as the interaction of individual spins with their respective external magnetic fields J_1 , while H_2 is the usual ZZ-interaction in the Ising model. Diagrammatically, this Hamiltonian can be depicted by the union of complete k -uniform hypergraphs ($k = 1, 2, \dots, N$) where the vertices denote the spins and the hyperedges denote the couplings between them.

To simplify the model, we can set the magnitudes of all the J_k to be the same, i.e. $|J_k| = J$, $k = 1, 2, \dots, n$. By choosing the signs appropriately, the energy spectrum can be made such that there is one ground state and $(N - 1)$ degenerate excited states, with an energy gap of NJ . Thus, by knowing the theoretically optimal energy gap $\epsilon(T_{\min}, T_{\max})$, one can tune $J = \epsilon/N$ to obtain the optimal probe for the Phase 1 thermometry. Interestingly, our numerical evidence suggests that the optimal energy structure in other phases can also be obtained with this generalized model (more details in Supplementary Note 2).

Although one could achieve the theoretical limits of equilibrium quantum thermometry with the classical Hamiltonian in Eq. (5), this generalized model is unrealistic since it requires full control of arbitrary k -body interactions. This is clearly not feasible for a reasonably large n . In the following subsection, we discuss the optimal global thermometry in realistic spin chain setups with much fewer control parameters.

Spin chain probes. As mentioned above, the optimal probes for global thermometry demand special form of energy structures, which are difficult to engineer with physical systems. Moreover, even if such spectra can be engineered, it might be challenging to measure the probe in the energy basis which is required to saturate the Cramér-Rao bound. Hence, there is a need to design practical probes with a high thermometric performance (compared to the theoretical limit). In this section, instead of optimizing over all the $(N - 1)$ independent energy levels, we first start with a spin chain system and minimize G over the spin chain parameters which can be controlled experimentally.

Restricting ourselves to 1D spin chains with only nearest-neighbour (two-body) interactions and periodic boundary conditions, we can write down a non-uniform Heisenberg XYZ Hamiltonian:

$$H_{\text{XYZ}} = \sum_{i=1}^n (J_x^i \sigma_x^i \sigma_x^{i+1} + J_y^i \sigma_y^i \sigma_y^{i+1} + J_z^i \sigma_z^i \sigma_z^{i+1}) + \sum_{i=1}^n (h_x^i \sigma_x^i + h_y^i \sigma_y^i + h_z^i \sigma_z^i) \quad (7)$$

with the presence of local external magnetic fields in all three directions. The couplings and fields are also allowed to vary independently throughout the spin chain. A further constraint $J_x^i = J_y^i = J_z^i = J^i$ can be added, which gives the non-uniform

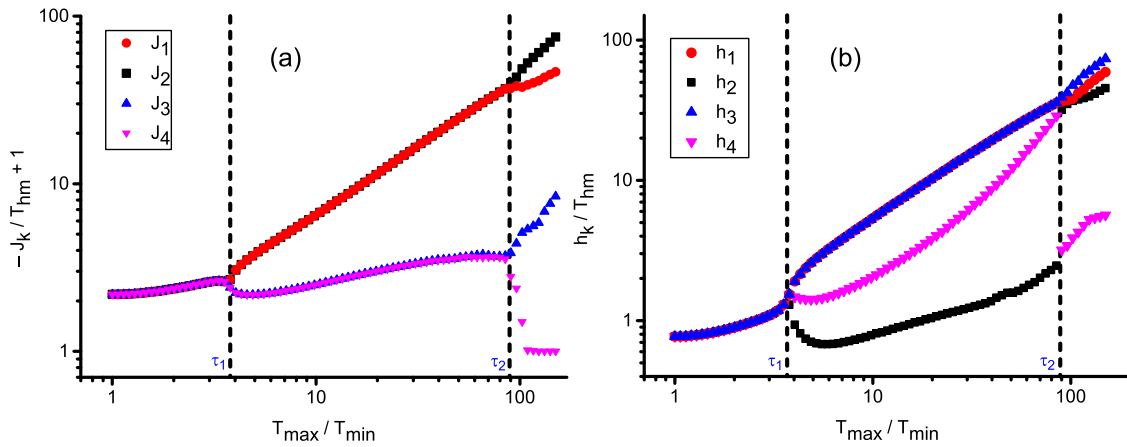


Fig. 2 Optimal probe for the non-uniform XYZ Hamiltonian. Optimal parameters against temperature ratio T_{\max}/T_{\min} for an optimized H_{XYZ} (reduced to an Ising model) for $n = 4$ spins. **a** ZZ-coupling strengths J_k between the k th and $(k+1)$ th spin ($k = 1, 2, 3, 4$). For illustration purposes, we plot $-J_k$ shifted positively by 1 unit. **b** External magnetic fields, with strength h_k acting on the k th spin. The parameters are scaled with the characteristic temperature T_{hm} , where T_{hm} is the harmonic mean of T_{\min} and T_{\max} . The dashed lines indicate the onset of the splitting of optimal parameters.

Heisenberg XXX Hamiltonian:

$$H_{\text{XXX}} = \sum_{i=1}^n J^i (\sigma_x^i \sigma_x^{i+1} + \sigma_y^i \sigma_y^{i+1} + \sigma_z^i \sigma_z^{i+1}) + \sum_{i=1}^n (h_x^i \sigma_x^i + h_y^i \sigma_y^i + h_z^i \sigma_z^i) \quad (8)$$

In practice, it is difficult to engineer exchange couplings with varying signs. Therefore, we impose the constraint that the spin chain probe must either be antiferromagnetic (all $J > 0$) or ferromagnetic (all $J < 0$), while the signs of the local magnetic fields can be arbitrarily varied. In the following, we numerically optimize H_{XYZ} and H_{XXX} for global quantum thermometry.

Special case: XYZ probe. As before, we minimize the average variance $G(T_{\min}, T_{\max})$ for various T_{\min} and T_{\max} over the parameters in H_{XYZ} . Interestingly, the optimization yields the classical (longitudinal-field) Ising model with $J_x = J_y = h_x = h_y = 0$ (omitting the spin indices). Having the Ising probe as the optimal solution also means that the same results would apply for the Heisenberg XXZ model as well. Figure 2a, b shows the optimal Ising couplings and magnetic fields obtained from H_{XYZ} for $n = 4$ spins. For thermometry in Phase 1, it turns out that the optimal solution is a uniform ferromagnetic Ising model with $J_z^i = -J < 0$ and $h_z^i = h > 0$ (see Supplementary Note 3). We note that the solution is not unique, and an antiferromagnetic Ising model with $J_z^i = J > 0$ is also possible with a different h_z^i . Interestingly, at the critical ratios indicated by the dashed lines, the uniformity of the optimal parameters breaks down, and the optimal parameters show a more sophisticated pattern.

Special case: XXX probe. For the XXX probe, for the sake of simplicity, we first impose another constraint on H_{XXX} by setting a homogenous magnetic field in each direction, i.e. $h_x^i = h_x$, $h_y^i = h_y$, $h_z^i = h_z \forall i$. Surprisingly, the optimal probe in this case turns out to be a fully dimerized spin chain with $J^i > 0$ for odd i and $J^i = 0$ otherwise. The optimal solutions require no external magnetic field ($h_x = h_y = h_z = 0$). Figure 3 shows the optimal couplings for the dimer chain obtained from H_{XXX} , for $n = 6$ spins. This gives us three independent dimers with coupling parameters J_1, J_2 and J_3 . In Phase 1, the dimers are all identical to one another. Again, at the critical ratios denoted by the dashed lines, the coupling parameters split into multiple branches.

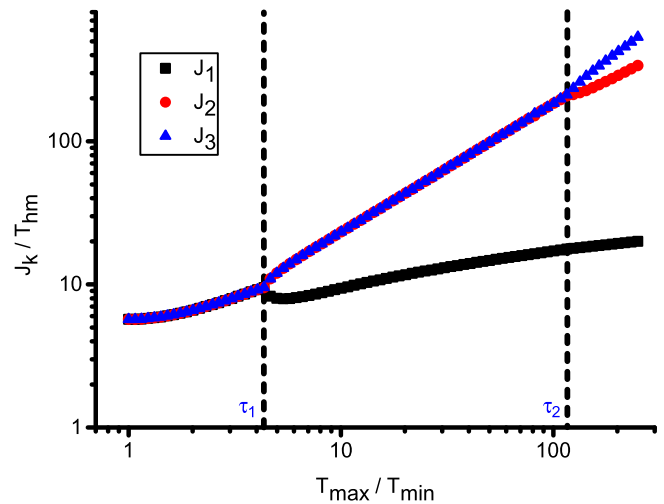


Fig. 3 Optimal probe for the non-uniform XXX Hamiltonian. Optimal coupling parameters J_k within the k th dimer ($k = 1, 2, 3$) against temperature ratio T_{\max}/T_{\min} for an optimized H_{XXX} (reduced to a dimerized chain) for $n = 6$ spins. The coupling parameters are scaled with the characteristic temperature T_{hm} , where T_{hm} is the harmonic mean of T_{\min} and T_{\max} . The dashed lines indicate the onset of the splitting of optimal parameters.

One can physically explain why the fully dimerized spin chain is the optimal solution for H_{XXX} . In the absence of external magnetic fields, the Heisenberg XXX Hamiltonian commutes with the total spin operator $\hat{S}^2 \equiv \hat{S}_x^2 + \hat{S}_y^2 + \hat{S}_z^2$. Hence, the first excited state has total spin = 1 and is triply-degenerate for all even values of n . By a similar symmetry argument, the uniform dimerized chain gives a $3n/2$ -fold degeneracy in the first excited state (see Fig. 4a for the example of $n = 2$), which is the maximum attainable value for the XXX Hamiltonian. That is why the fully dimerized chain becomes the optimal probe in Phase 1. As new phases emerge, one of the couplings of the dimers changes to vary the degeneracy of the spectrum, replicating the bifurcations found for the optimal probes. It is also noted that if we relax the constraint of homogeneous magnetic fields in H_{XXX} , we obtain a probe that is only marginally better than the dimerized chain.

Optimal measurements. In general, energy measurements is very difficult in practice, making the saturation of Cramér-Rao bound

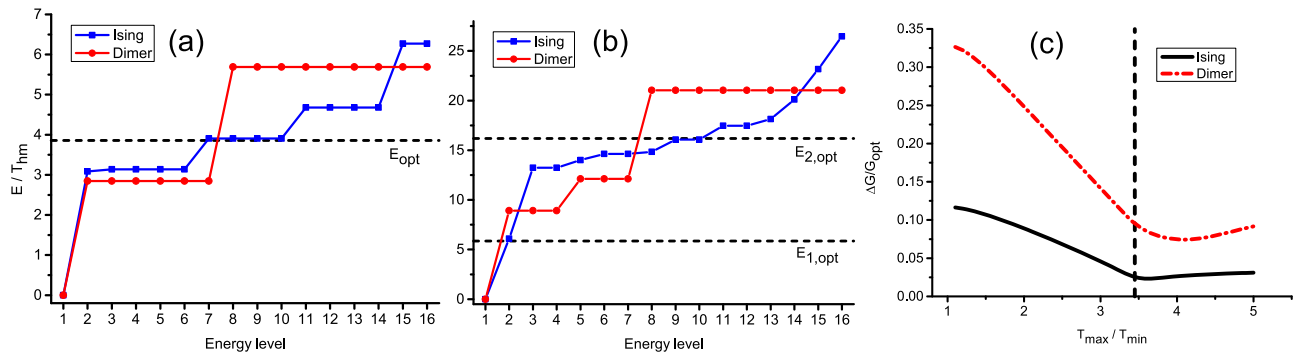


Fig. 4 Comparison of global thermometers. Comparison of energy levels between the Ising model (blue squares, obtained from optimizing the XYZ Hamiltonian H_{XYZ}) and the dimerized chain (in red circles, obtained from optimizing the XYZ Hamiltonian H_{XXX}). The energy levels are normalized against T_{hm} , the harmonic mean of T_{\min} and T_{\max} (the lower and upper bounds of the temperature range respectively). The number of spins is $n = 4$ (corresponding to $N = 2^n = 16$ energy levels), and the optimal energies (dashed lines) are calculated for two different temperature ratios: **a** $T_{\max}/T_{\min} = 1$ (corresponding to Phase 1 in Fig. 1b). E_{opt} indicates the optimal energy level for the excited state. **b** $T_{\max}/T_{\min} = 5$ (corresponding to Phase 2 in Fig. 1b). $E_{1,\text{opt}}$ and $E_{2,\text{opt}}$ indicate the optimal energy level for the first and second excited states, respectively. The Ising energy levels are on average of closer proximity to the optimal energies. **c** Relative difference in the global thermometry measure G against temperature ratio T_{\max}/T_{\min} for the Ising model (black solid line, obtained from optimizing H_{XYZ}) and the dimerized chain (red dash-dotted line, obtained from optimizing H_{XXX}). G_{opt} is the theoretical lower bound for the G value. The number of spins is $n = 4$, compared to the ideal case with $N = 16$ energy levels. The dashed line indicate the critical ratio for the ideal probe.

challenging. Remarkably, the probes obtained from optimizing H_{XYZ} and H_{XXX} are not just solutions that minimize G , but also have the added advantage of being easily measurable in the energy basis. In the case of H_{XYZ} where the longitudinal-field Ising model is optimal, the energy measurements are equivalent to measuring all the spins in the computational basis, i.e. σ_z , which has been realized in various physical setups^{56,57}. In the case of H_{XXX} where the fully dimerized chain is the optimal probe, the energy measurements is reduced to a series of singlet-triplet measurements on all the dimer pairs, which is a typical measurement in quantum dot arrays^{58,59}.

Thus, the optimization results discussed earlier can saturate the Cramér-Rao bound on top of having a low G .

Comparison with theoretical limit. It is insightful to study the energy spectra of the optimized spin chain probes for H_{XYZ} and H_{XXX} . For optimal probes of size $n = 4$, we plot in Fig. 4a, b the energy spectra for $T_{\max}/T_{\min} = 1$ (Phase 1) and $T_{\max}/T_{\min} = 5$ (Phase 2), respectively. For Phase 1, the Ising excited energy levels shown in Fig. 4a are on average closer to the optimal energy E_{opt} , denoted by the dashed line. Likewise, considering the case of Phase 2 thermometry in Fig. 4b, the Ising energy levels are closer to the respective optimal energies $E_{1,\text{opt}}$ (degeneracy = 1) and $E_{2,\text{opt}}$ (degeneracy = $N - 2$). In particular, we see that the Ising model has a single first excited state very close to $E_{1,\text{opt}}$, whereas the first excited state of the dimer must be threefold degenerate. This suggests that the Ising probe performs better than the dimerized probe in both cases. This is not surprising since H_{XYZ} is more general than H_{XXX} , so we must always have $G_{\text{Ising}} \leq G_{\text{dimer}}$.

In order to quantify the quality of the optimal spin chain probes, one has to compare their performance with the theoretically ideal thermometers. To do so, we compute the relative difference in G with G_{opt} , i.e. $\Delta G/G_{\text{opt}} \equiv G/G_{\text{opt}} - 1$ for probes with $n = 4$, over a range of T_{\max}/T_{\min} for which two phases are observable. When ΔG is small, it means that the probes perform closer to the theoretical limit. The results are plotted in Fig. 4c. Remarkably, the Ising and dimerized probes perform closer to the theoretical limit in Phase 2 as compared to Phase 1. In addition, as expected, the Ising probe indeed outperforms the dimerized probe at all values of T_{\max}/T_{\min} .

In summary, we quantitatively formalize the notion of global thermometry, which operates over arbitrary large temperature ranges. This is achieved by minimizing the average of variance over a given temperature interval. The proposed approach naturally provides the energy structure of an optimal probe. Interestingly, depending on the temperature range, the optimal thermometer goes through different phases, each favouring a particular energy structure. We note that an alternative formulation for the theory of global quantum thermometry was also recently proposed by Rubio et al.⁶⁰, which treats it as a scale estimation problem. However, in their example the physical system is a gas of fermions with identical energies, hence they were unable to observe the bifurcation of energy levels that we discovered.

We provide a realization of such optimal probes in generalized Ising models with multi-particle interactions. In practice, however, such interactions might be challenging to fabricate. Hence, by imposing further constraints, we provide new designs for optimal probes which are limited to two-body interactions in the form of nearest neighbours of special type of interactions. Starting from a non-uniform XYZ Hamiltonians, our optimization results in a uniform Ising model as the optimal thermometer which can be realized in ion traps. On the other hand, if we restrict ourselves to non-uniform Heisenberg models, then the optimal thermometer is a dimerized chain which can be realized in quantum dot arrays. We also observe the appearance of various phases for practically optimal probes as we vary the temperature range.

Our results unlock several fresh research avenues. For instance, how one can generalize the developed global thermometry procedure to non-equilibrium probes. Another direction to pursue is to find optimal designs for thermometers in other physical platforms, such as optomechanical systems or itinerant particles.

Methods

The numerical optimization in this work is done primarily using global optimization routines. In particular, we use the SciPy implementation⁶¹ of differential evolution⁶², which is an example of an evolutionary algorithm. Differential evolution is a metaheuristic search algorithm that iteratively improves the candidate solution by evolving the population which navigates the search space. It does not rely on gradient information, making it suitable for exploring large search spaces which is useful for optimizing over large number of energy levels. In all cases, we

use a population of 500, and increasing the population further does not improve the quality of the optimal solution found. The results are also verified with other popular global optimization routines such as simulated annealing and basin-hopping. Hence, our results do not depend on the specific optimization algorithm used.

For spin chains with $n \geq 10$, global optimization becomes infeasible due to two sources of computational costs: (i) diagonalization of the Hamiltonian (in an exponentially large Hilbert space) to obtain all the eigenenergies at each step, and (ii) large number of iterations required for global optimization. While it is possible to speed up the computation by restricting the diagonalization to only return a subset of the lowest eigenenergies, we found that the optimal results are rather inaccurate unless most of the eigenvalues are retained. Hence, the speed up from this approach is marginal. In order to proceed with the optimization for larger systems, we employ a transfer learning approach where the optimal probe for a smaller N is recursively used as an initial guess for an incrementally larger system size, and perform local optimization using the gradient-based BFGS algorithm (see Supplementary Note 3).

Data availability

The data that support the plots within this paper are available upon reasonable request.

Received: 25 November 2020; Accepted: 8 March 2021;

Published online: 25 March 2021

References

- Degen, C. L., Reinhard, F. & Cappellaro, P. Quantum sensing. *Rev. Mod. Phys.* **89**, 035002 (2017).
- Giovannetti, V., Lloyd, S. & Maccone, L. Quantum-enhanced measurements: beating the standard quantum limit. *Science* **306**, 1330–1336 (2004).
- Huang, Z., Macchiavello, C. & Maccone, L. Cryptographic quantum metrology. *Phys. Rev. A* **99**, 022314 (2019).
- Bloch, I., Dalibard, J. & Zwierger, W. Many-body physics with ultracold gases. *Rev. Mod. Phys.* **80**, 885 (2008).
- Giazotto, F., Heikkilä, T. T., Luukanen, A., Savin, A. M. & Pekola, J. P. Opportunities for mesoscopes in thermometry and refrigeration: physics and applications. *Rev. Mod. Phys.* **78**, 217 (2006).
- Vinjanampathy, S. & Anders, J. Quantum thermodynamics. *Contemp. Phys.* **57**, 545–579 (2016).
- Mehboudi, M., Sanpera, A. & Correa, L. A. Thermometry in the quantum regime: recent theoretical progress. *J. Phys. A* **52**, 303001 (2019).
- Binder, F., Correa, L. A., Gogolin, C., Anders, J. & Adesso, G. Thermodynamics in the quantum regime. *Fundamental Theories Phys.* **195**, 1–2 (2018).
- Campisi, M., Hänggi, P. & Talkner, P. Colloquium: quantum fluctuation relations: foundations and applications. *Rev. Mod. Phys.* **83**, 771–791 (2011).
- Perarnau-Llobet, M., Bäumer, E., Hovhannisyan, K. V., Huber, M. & Acín, A. No-go theorem for the characterization of work fluctuations in coherent quantum systems. *Phys. Rev. Lett.* **118**, 070601 (2017).
- Talkner, P. & Hänggi, P. Aspects of quantum work. *Phys. Rev. E* **93**, 022131 (2016).
- Esposito, M., Lindenberg, K. & Van den Broeck, C. Entropy production as correlation between system and reservoir. *New J. Phys.* **12**, 013013 (2010).
- Brandao, F., Horodecki, M., Ng, N., Oppenheim, J. & Wehner, S. The second laws of quantum thermodynamics. *Proc. Natl. Acad. Sci. USA* **112**, 3275–3279 (2015).
- Uzdin, R. & Rahav, S. Global passivity in microscopic thermodynamics. *Phys. Rev. X* **8**, 021064 (2018).
- Kolář, M., Gelbwaser-Klimovsky, D., Alicki, R. & Kurizki, G. Quantum bath refrigeration towards absolute zero: challenging the unattainability principle. *Phys. Rev. Lett.* **109**, 090601 (2012).
- Levy, A., Alicki, R. & Kosloff, R. Quantum refrigerators and the third law of thermodynamics. *Phys. Rev. E* **85**, 061126 (2012).
- Bayat, A. et al. Nonequilibrium critical scaling in quantum thermodynamics. *Phys. Rev. B* **93**, 201106 (2016).
- Degen, C. L., Reinhard, F. & Cappellaro, P. Quantum sensing. *Rev. Mod. Phys.* **89**, 035002 (2017).
- He, J., Chen, J. & Hua, B. Quantum refrigeration cycles using spin-1/2 systems as the working substance. *Phys. Rev. E* **65**, 036145 (2002).
- Timofeev, A. V., Helle, M., Meschke, M., Möttönen, M. & Pekola, J. P. Electronic refrigeration at the quantum limit. *Phys. Rev. Lett.* **102**, 200801 (2009).
- Mohammady, M. H. et al. Low-control and robust quantum refrigerator and applications with electronic spins in diamond. *Phys. Rev. A* **97**, 042124 (2018).
- Sone, A., Cerezo, M., Beckey, J. L. & Coles, P. J. A generalized measure of quantum fisher information. Preprint at <https://arxiv.org/abs/2010.02904> (2020).
- Beckey, J. L., Cerezo, M., Sone, A. & Coles, P. J. Variational quantum algorithm for estimating the quantum fisher information. Preprint at <https://arxiv.org/abs/2010.10488> (2020).
- Toyli, D. M., Charles, F., Christle, D. J., Dobrovitski, V. V. & Awschalom, D. D. Fluorescence thermometry enhanced by the quantum coherence of single spins in diamond. *Proc. Natl. Acad. Sci. USA* **110**, 8417–8421 (2013).
- Kucsko, G. et al. Nanometre-scale thermometry in a living cell. *Nature* **500**, 54–58 (2013).
- Grover, J., Solano, P., Orozco, L. & Rolston, S. Photon-correlation measurements of atomic-cloud temperature using an optical nanofiber. *Phys. Rev. A* **92**, 013850 (2015).
- Purdy, T., Grutter, K., Srinivasan, K. & Taylor, J. Quantum correlations from a room-temperature optomechanical cavity. *Science* **356**, 1265–1268 (2017).
- Stace, T. M. Quantum limits of thermometry. *Phys. Rev. A* **82**, 011611 (2010).
- Potts, P. P., Brask, J. B. & Brunner, N. Fundamental limits on low-temperature quantum thermometry with finite resolution. *Quantum* **3**, 161 (2019).
- Brunelli, M., Olivares, S. & Paris, M. G. Qubit thermometry for micromechanical resonators. *Phys. Rev. A* **84**, 032105 (2011).
- Brunelli, M., Olivares, S., Paternostro, M. & Paris, M. G. Qubit-assisted thermometry of a quantum harmonic oscillator. *Phys. Rev. A* **86**, 012125 (2012).
- Sabín, C., White, A., Hackermüller, L. & Fuentes, I. Impurities as a quantum thermometer for a bose-einstein condensate. *Sci. Rep.* **4**, 1–6 (2014).
- Mehboudi, M., Moreno-Cardoner, M., De Chiara, G. & Sanpera, A. Thermometry precision in strongly correlated ultracold lattice gases. *New J. Phys.* **17**, 055020 (2015).
- Guo, L.-S., Xu, B.-M., Zou, J. & Shao, B. Improved thermometry of low-temperature quantum systems by a ring-structure probe. *Phys. Rev. A* **92**, 052112 (2015).
- Hofer, P. P., Brask, J. B., Perarnau-Llobet, M. & Brunner, N. Quantum thermal machine as a thermometer. *Phys. Rev. Lett.* **119**, 090603 (2017).
- De Pasquale, A., Yuasa, K. & Giovannetti, V. Estimating temperature via sequential measurements. *Phys. Rev. A* **96**, 012316 (2017).
- Campbell, S., Mehboudi, M., De Chiara, G. & Paternostro, M. Global and local thermometry schemes in coupled quantum systems. *New J. Phys.* **19**, 103003 (2017).
- Campbell, S., Genoni, M. G. & Deffner, S. Precision thermometry and the quantum speed limit. *Quantum Sci. Technol.* **3**, 025002 (2018).
- Plodzień, M., Demkowicz-Dobrzański, R. & Sowiński, T. Few-fermion thermometry. *Phys. Rev. A* **97**, 063619 (2018).
- Sone, A., Zhuang, Q. & Cappellaro, P. Quantifying precision loss in local quantum thermometry via diagonal discord. *Phys. Rev. A* **98**, 012115 (2018).
- Montenegro, V., Genoni, M. G., Bayat, A. & Paris, M. G. A. Mechanical oscillator thermometry in the nonlinear optomechanical regime. *Phys. Rev. Res.* **2**, 043338 (2020).
- Feyles, M. M., Mancino, L., Sbroscia, M., Gianani, I. & Barbieri, M. Dynamical role of quantum signatures in quantum thermometry. *Phys. Rev. A* **99**, 062114 (2019).
- Gebbia, F. et al. Two-qubit quantum probes for the temperature of an ohmic environment. *Phys. Rev. A* **101**, 032112 (2020).
- Mancino, L., Genoni, M. G., Barbieri, M. & Paternostro, M. Nonequilibrium readiness and precision of Gaussian quantum thermometers. *Phys. Rev. Res.* **2**, 033498 (2020).
- Mitchison, M. T. et al. In situ thermometry of a cold fermi gas via dephasing impurities. *Phys. Rev. Lett.* **125**, 080402 (2020).
- Mukherjee, V., Zwick, A., Ghosh, A., Chen, X. & Kurizki, G. Enhanced precision bound of low-temperature quantum thermometry via dynamical control. *Commun. Phys.* **2**, 1–8 (2019).
- Seah, S. et al. Collisional quantum thermometry. *Phys. Rev. Lett.* **123**, 180602 (2019).
- Mancino, L., Genoni, M. G., Barbieri, M. & Paternostro, M. Nonequilibrium readiness and precision of Gaussian quantum thermometers. *Phys. Rev. Res.* **2**, 033498 (2020).
- Mondal, S., Bhattacharjee, S. & Dutta, A. Exploring the role of asymmetric-pulse modulation in quantum thermal machines and quantum thermometry. *Phys. Rev. E* **102**, 022140 (2020).
- Correa, L. A., Mehboudi, M., Adesso, G. & Sanpera, A. Individual quantum probes for optimal thermometry. *Phys. Rev. Lett.* **114**, 220405 (2015).
- Paris, M. G. Achieving the landau bound to precision of quantum thermometry in systems with vanishing gap. *J. Phys. A* **49**, 03LT02 (2015).
- Correa, L. A. et al. Enhancement of low-temperature thermometry by strong coupling. *Phys. Rev. A* **96**, 062103 (2017).
- De Pasquale, A., Rossini, D., Fazio, R. & Giovannetti, V. Local quantum thermal susceptibility. *Nat. Commun.* **7**, 1–8 (2016).

54. Razavian, S. & Paris, M. G. Quantum metrology out of equilibrium. *Phys. A* **525**, 825–833 (2019).
55. Cramér, H. *Mathematical Methods of Statistics*, Vol. 43 (Princeton University Press, 1999).
56. O'Malley, P. J. J. et al. Scalable quantum simulation of molecular energies. *Phys. Rev. X* **6**, 031007 (2016).
57. Kokail, C. et al. Self-verifying variational quantum simulation of lattice models. *Nature* **569**, 355–360 (2019).
58. Petta, J. R. et al. Coherent manipulation of coupled electron spins in semiconductor quantum dots. *Science* **309**, 2180–2184 (2005).
59. Fogarty, M. A. et al. Integrated silicon qubit platform with single-spin addressability, exchange control and single-shot singlet-triplet readout. *Nat. Commun.* **9**, 4370 (2018).
60. Rubio, J., Anders, J. & Correa, L. A. Global quantum thermometry. Preprint at <https://arxiv.org/abs/2011.13018> (2020).
61. Virtanen, P. et al. SciPy 1.0: fundamental algorithms for scientific computing in Python. *Nat. Methods* **17**, 261–272 (2020).
62. Storn, R. & Price, K. Differential evolution as a simple and efficient heuristic for global optimization over continuous spaces. *J. Glob. Optim.* **11**, 341–359 (1997).

Acknowledgements

A.B. acknowledges the National Key R&D Program of China, Grant No. 2018YFA0306703. K.B. and L.C.K. are grateful to the National Research Foundation and the Ministry of Education, Singapore for financial support. The authors thank Jingu Pang for the drawing of the schematic diagram.

Author contributions

The idea of the paper was conceived through discussions between all the authors. W.K.M. performed the numerical simulations. W.K.M., K.B., K.L.C. and A.B. wrote the paper, and discussed the methodology, results and implications at all stages.

Competing interests

The authors declare no competing interests.

Additional information

Supplementary information The online version contains supplementary material available at <https://doi.org/10.1038/s42005-021-00572-w>.

Correspondence and requests for materials should be addressed to A.B.

Reprints and permission information is available at <http://www.nature.com/reprints>

Publisher's note Springer Nature remains neutral with regard to jurisdictional claims in published maps and institutional affiliations.



Open Access This article is licensed under a Creative Commons Attribution 4.0 International License, which permits use, sharing, adaptation, distribution and reproduction in any medium or format, as long as you give appropriate credit to the original author(s) and the source, provide a link to the Creative Commons license, and indicate if changes were made. The images or other third party material in this article are included in the article's Creative Commons license, unless indicated otherwise in a credit line to the material. If material is not included in the article's Creative Commons license and your intended use is not permitted by statutory regulation or exceeds the permitted use, you will need to obtain permission directly from the copyright holder. To view a copy of this license, visit <http://creativecommons.org/licenses/by/4.0/>.

© The Author(s) 2021